The effect of initial velocity on rotational energy transfer in 13CH3F

Quan Song and R. H. Schwendeman

Citation: The Journal of Chemical Physics **98**, 9472 (1993); doi: 10.1063/1.465083
View online: http://dx.doi.org/10.1063/1.465083
View Table of Contents: http://scitation.aip.org/content/aip/journal/jcp/98/12?ver=pdfcov
Published by the AIP Publishing

The effect of initial velocity on rotational energy transfer in $^{13}CH_3F$

Quan Song and R. H. Schwendeman
Department of Chemistry, Michigan State University, East Lansing, Michigan 48824

(Received 25 January 1993; accepted 1 March 1993)

The dependence on initial velocity of collisionally-induced rotational transitions in CH_3F has been studied by infrared–infrared four-level double resonance experiments in which the offset of the pump laser was varied in order to vary the velocity component in the direction of the pump beam of the excited molecules. For this purpose, the frequency of the carbon dioxide pump laser was stabilized to a saturation dip (Lamb dip) in the Stark spectrum in a CH_3F sample in a cell outside the laser cavity, which provided a tunability of $\sim$30 MHz for each laser line. It was found that the rms change in a velocity component during collisionally-induced transitions is roughly proportional to the rms relative speed of the colliding molecules. Velocity dependence of the rates of rotational energy transfer has also been observed. Classical elastic scattering theory has been used to calculate the one-dimensional collision kernel at different initial values of the component of the velocity of the active molecule in the direction of the beam. The results of this calculation do not agree with the qualitative features of the observation.

I. INTRODUCTION

Infrared–infrared double resonance has proved to be a powerful tool for the study of velocity-changing collisions. Because the Doppler width in the mid-infrared region is large compared to both the available resolution and the inhomogeneous width for low-pressure gases, a strong monochromatic infrared laser can prepare molecules in a specific rovibrational state with a specific velocity component in the direction of the radiation. A second monochromatic, but continuously tunable infrared laser can then provide detailed information about the correlation between velocity change and state change upon collision. Infrared–infrared double resonance experiments employing this concept, or the closely related techniques of Stark tuning and Lamb dips, were first carried out by Freund *et al.*,[1] by Meyer and Rhodes,[2] by Brewer *et al.*,[3] and by Johns *et al.*[4] In these and subsequent studies the qualitative features of the velocity change as a result of collision were described and many of the characteristics of such velocity changes were identified and treated theoretically. However, relatively little quantitative information was obtained, especially for the case in which the rotational angular momentum was changed by the collisions.

Recently, quantitative characterizations of the velocity changes during rotational energy transfer were reported for $^{15}NH_3$ and $^{13}CH_3F$ by Matsuo *et al.*,[5,6] and then for $^{12}CH_3F$ by Shin *et al.*[7] from this laboratory. In these studies, a single transition in a fundamental vibration-rotation band was pumped by radiation from a single-mode CO_2 laser while a transition in a hot band was probed by a tunable infrared microwave sideband laser source. The uniqueness of the experimental strategy was that the pumping power was relatively low (cw CO_2 laser), which guaranteed the excitation of molecules with a narrow velocity distribution, and the probe source was highly monochromatic, which made it possible to examine the detailed velocity distribution after collision as well as the relative intensity of the effects on the line shapes of different contributions to the collisionally induced energy transfer. Thus, this work was complementary to the work mentioned earlier and to time-resolved infrared–infrared double resonance experiments employing a pulsed high-power pump laser and a relatively low resolution probe source (e.g., an infrared diode laser), such as the studies reported by Steinfeld's group,[8–11] in which the pumping power density was so high that the power broadening was sufficient to cause pumping of nearly all velocity groups.

In the recent experiments from this laboratory,[5–7] the line shape of the probing transition was found to be a superposition of a broad Gaussian and a sharp spike. The Gaussian component was interpreted to be the result of near resonant vibration–vibration (V–V) energy transfer, in which the pumped molecule swapped vibrational energy with a molecule in the ground vibrational state. In this process, the molecules transferred to the probed level are not the molecules that are pumped. The molecules transferred come from a near thermal equilibrium distribution so that the resulting contribution to the probe transition is a Gaussian function with the expected Doppler width. The spike component was assumed to be the result of direct collisionally-induced transitions, where the pumped molecules find themselves at the lower state of the probe as a result of collisions. Since the pumped molecules have a very narrow distribution of the velocity component in the direction of the beam and the collisionally-induced transitions occur without much change in velocity for the system investigated, the resulting contribution to the line shape of the probe transition is a sharp spike.

In the experiments just described, the spike components were observed only when the K quantum numbers of the lower level of the probe transition and the upper level of the pump transition satisfied the selection rule $K(\text{probe}) - K(\text{pump}) = 3n$, where n is a positive or negative integer

 0021-9606/93/129472-09$06.00

or zero. This selection rule was observed first by Oka,[12,13] and then by a number of other authors,[5–7,9,14–16] for collisionally-induced rotational transitions in C_{3v} molecules. In our laboratory, it was found that a phenomenological collision kernel that was a sum of two Keilson and Storer (KS) kernels,[17] represented the velocity changes during the collisionally-induced transition very well. One of the parameters in the KS kernel can be interpreted to be the rms change in velocity upon collision. By numerical fitting of the theoretical line shape obtained from the phenomenological kernel to the observed spectrum, values of the rms velocity change upon collision were determined.

The previous studies from this laboratory provided experimental observations of the transferred spikes and laid a theoretical foundation for analysis of the transferred spikes to extract information about the velocity change during the collisionally-induced transitions. In the present work we describe the results of experiments performed to determine dependence on initial velocity of the characteristics of collisionally-induced rotational energy transfer in $^{13}CH_3F$. One of the major motivations of this work was to investigate the velocity dependence of the phenomenological collision kernel that has been used to obtain the root-mean-square velocity change upon collision from four-level infrared–infrared double resonance line shapes.[5–7] The KS kernel has been used in various collisional problems[2,3,5–7,18–22] and the parameter representing the rms velocity change in the kernel was known to be dependent on the collisional interaction, relative masses, and relative velocity of the colliding pair. In addition, from a practical point of view, knowledge of the velocity dependence of the parameter is essential in order to simulate the collision process (i.e., determine the final velocity distribution) with the kernel for molecules that have an initial velocity distribution instead of a single velocity.

The velocity component of the molecules pumped by a coincident laser in the direction of the laser beam is determined by the Doppler effect and can be varied by changing the pump laser frequency (or pump laser offset). Smith *et al.* have used this concept to carry out a series of measurements of velocity dependences of rates for rotational energy transfer in Na_2 and Li_2 colliding with rare-gas atoms.[23–25] In these experiments, the pump transitions were in the visible region where the well-developed continuously tunable dye laser can change the pump laser frequency easily. Study of the velocity dependence of a collisional process by means of velocity selection by Doppler shift is probably more difficult in the infrared region than in the visible region. Besides the fact that a strong and continuously tunable infrared laser is hard to find, the absolute frequency stability of the pump laser required for the same velocity resolution is more rigorous in the infrared region than in the visible region. This is because the Doppler shift in frequency for a molecule with a given velocity is proportional to the frequency of the transition. Thus, a change in the frequency of the radiation has a smaller effect on the velocity when the frequency is larger. Nevertheless, Mattick *et al.* investigated the velocity dependence of collisional broadening in an infrared transition in NH_3.[26]

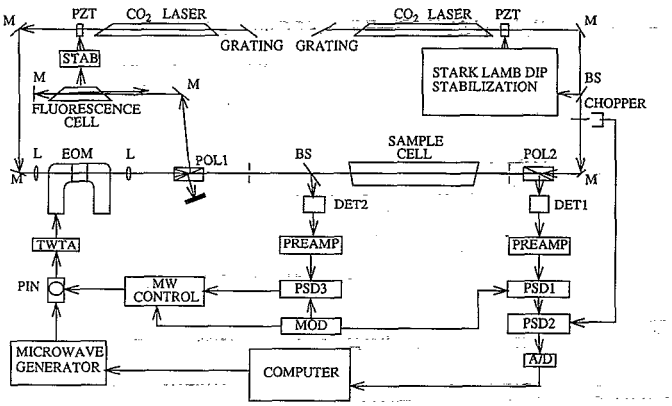

FIG. 1. Block diagram of infrared–infrared double resonance spectrometer. M=mirror; L=lens; BS=beam splitter; PZT=piezoelectric translator and output coupler; EOM=electro-optic modulator; POL1, POL2 =polarizers; DET1, DET2=infrared detectors; MOD=function generator.

In order to study the velocity dependence of rotational energy transfer in CH_3F by infrared–infrared double resonance, we had to have a pump source that was both tunable and very monochromatic. For this purpose, we stabilized the pump laser (a CO_2 laser) to a saturation dip (Lamb dip) in the Stark spectrum of $^{13}CH_3F$ in a cell outside of the laser cavity. This technique was used by Grossman *et al.*[27] and by Weber and Terhune[28] to stabilize CO_2 and CO laser frequencies, respectively. The advantage of this stabilization scheme, in addition to the extremely high frequency stability, is the ability to stabilize the laser line at any frequency within the laser gain curve, and therefore, to provide the necessary tunability for pumping molecules in different velocity groups.

In order to see how the classical elastic scattering theory describes the velocity dependence of the rms velocity change during collision for a Lennard-Jones molecular potential function, we used a Monte Carlo calculation, described in more detail in Ref. 29, to simulate collisional processes with two different initial velocities of active molecules. Although the simulation also showed a velocity dependence of the rms velocity change during collision, the calculated variation was opposite to that observed in experiment. The disagreement between the observed and calculated results will be discussed.

II. EXPERIMENTAL DETAILS

Figure 1 is a block diagram of the infrared–infrared double resonance spectrometer used in this work. Except for the pump laser stabilization, the spectrometer was the same as that used in previous work from this laboratory.[5–7] The pump source was a single-mode flowing gas CO_2 laser that is useful for operating at high J laser lines. The probe source was an infrared microwave sideband system driven by a second CO_2 laser that uses a semi-sealed plasma tube and can be operated with an isotopic species of CO_2. The frequency of the CO_2 laser used for the sideband system was stabilized by means of a fluorescence Lamb dip from a

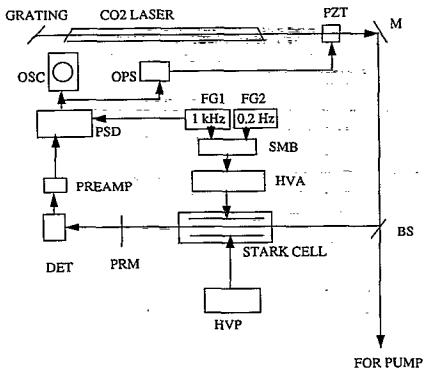

FIG. 2. Setup for stabilization of CO_2 laser to a Stark Lamb dip. M=mirror; PZT=piezoelectric translator and laser output coupling mirror; BS=beam splitter; FG1, FG2=function generators; SMB=signal mixer; HVA=high voltage amplifier; HVP=high voltage power supply; PRM=90% partially reflecting mirror; DET=detector; PREAMP =preamplifier; PSD=phase sensitive detector; OPS=operational power supply; OSC=oscilloscope.

CO_2 sample in a cell outside the laser cavity, as in our previous studies. The overall frequency stability for this laser and for the Stark-stabilized pump laser was $\sim\pm 150$ kHz. The probe laser was 100% amplitude modulated at 33 kHz by chopping the microwaves applied to the modulator crystal, while the pump laser beam was modulated at 150 Hz by means of a mechanical chopper. The polarizations of the pump and probe lasers were perpendicular to one another and the geometry of the two beams was counterpropagating. In order to stabilize the amplitude of the probe laser, a second detector was used to monitor the laser power in front of the sample cell. The output of this detector drives a feedback circuit which controls the microwave power applied to the modulator crystal so that any change in probe power will be compensated by an appropriate change in microwave power. Typical pump powers at the entrance of the sample cell were ~ 1 W, while probe powers were ~ 20 μW. The microwave frequency for the sideband laser is provided by a synthesizer (± 3 kHz accuracy) and is stepped by the microcomputer that records the spectrum.

Figure 2 shows the setup used for stabilizing the CO_2 pump laser to a Lamb dip in a Stark spectrum. A beam splitter directs a portion of the pump laser beam to a Stark cell outside the laser cavity. A mirror with 90% reflection and 10% transmission (PRM) is placed at the output of the Stark cell to reflect most of the beam back through the cell to form a typical structure for Lamb dip generation. Connected to one plate of the Stark cell is a high voltage power supply (HVP) which can be operated up to 2 kV at either positive or negative voltage. The other plate is connected to a high voltage amplifier (HVA) which provides a continuously variable source up to 10 kV at either polarity. To lock the laser, a strong saturation dip is first observed by superimposing a 10 kHz sine wave signal (from FG1) on a 0.2 Hz triangular wave (from FG2) by means of a signal mixing box (SMB) whose output is amplified 1000 times by the high voltage amplifier. The sine wave signal provides the necessary modulation of the Stark field while the triangular wave scans the high voltage so that the Lamb dip signal can be seen on an oscilloscope. For this purpose, the output of the infrared detector is amplified by a preamplifier and then demodulated at 10 kHz by a phase sensitive detector whose output is used for locking the laser. For stabilization, the high voltage is adjusted to the center of the Lamb dip, the triangular wave is turned off, and the voltage-amplified output of the phase-sensitive detector is applied to a piezoelectric translator attached to the end mirror of the laser.

A double modulation scheme is used to analyze the signal. The output of the signal detector is first demodulated by a lock-in amplifier at the chopping frequency of the probe; the output of this amplifier, which contains the sum of the single-resonance and double-resonance effects, is sent to a second lock-in amplifier for an additional demodulation at the chopping frequency of the pump laser. The output of the second amplifier, which contains only the double-resonance effect, is digitized and recorded by the microcomputer.

The pump laser power was carefully controlled and monitored in this study. Each time the pump offset was changed, the pumping power was measured before the sample cell and kept at the same level by rotating an additional polarizer in front of POL2 (Fig. 1) to change the amplitude of the horizontal component of the pumping radiation. The pumping power was also monitored from time to time and the fluctuation at the same offset was less than 3%.

The sample cell for this work was a Pyrex tube, 1 m long and 25 mm in diameter. The $^{13}CH_3F$ sample was obtained from Merck & Co. and, except for the usual freeze-pump-thaw cycling, was used as received. All spectra were recorded at room temperature (~ 297 K) at pressures of 10 mTorr; sample pressures were measured by a capacitance manometer. The frequencies for the pump and probe transitions and the lasers used are shown in Table I.

III. THEORETICAL SECTION

A. Relative velocity of the colliding molecules

In our experiment, the active molecules (the molecules pumped) have a fixed velocity component in the direction of the pump laser. All of the other velocity components of both the active molecules and the perturbers are assumed to be in an equilibrium distribution. If we choose a coordinate system so that the pump beam travels in the space-fixed z direction, the velocity component in the z direction for the active molecules can be calculated from the Doppler equation

$$v_z=\frac{c}{\nu_p^0}(\nu_l-\nu_p^0), \tag{1}$$

where c is the speed of light, ν_l is the frequency of the pump laser, and ν_p^0 is the center frequency of the pump transition. If only molecules with v_{az} equal to v_z given by Eq. (1) are pumped, then the probability of finding among these molecules an excited active molecule with velocity,

TABLE I. Pump and probe transitions used for double resonance in $^{13}CH_3F$.

Transition	Band	Frequency[a]	Offset[b]	Laser[c]
		Pump Transitions		
$^{Q}R(4,3)$	ν_3	31 042 693.8	8.6	$^{12}C^{16}O$ 9P(32)
$^{Q}R(4,3)$	ν_3	31 042 693.8	23.1	$^{12}C^{16}O$ 9P(32)
$^{Q}R(4,3)$	ν_3	31 042 693.8	37.8	$^{12}C^{16}O$ 9P(32)
		Probe Transitions		
$^{Q}P(5,3)$	$2\nu_3-\nu_3$	30 092 980.5	14 572.6	$^{13}C^{16}O$ 9P(16)
$^{Q}P(6,3)$	$2\nu_3-\nu_3$	30 040 821.2	12 707.4	$^{13}C^{16}O$ 9P(18)
$^{Q}P(7,3)$	$2\nu_3-\nu_3$	29 988 049.4	10 600.7	$^{13}C^{16}O$ 9P(20)
$^{Q}P(8,3)$	$2\nu_3-\nu_3$	29 934 667.0	8 253.7	$^{13}C^{16}O$ 9P(22)

[a]Center frequency of the transition in MHz determined in Refs. 30 and 32.

[b]The CO_2 laser frequency minus center frequency of the transition in MHz.

[c]Pump lasers were stabilized to the Stark Lamb dip of the $R(4,1)$, $m=5\leftarrow4$, transition in the ν_3 band of $^{13}CH_3F$; the electric field applied for Stark Lamb dips for different pump laser offsets were 7.851 kV/cm for 8.6 MHz; 8.363 kV/cm for 23.1 MHz; 8.875 kV/cm for 37.8 MHz. Probe lasers were stabilized to the fluorescence Lamb dip of a $^{13}C^{16}O_2$ sample.

$$\mathbf{v}_a=v_{ax}\mathbf{i}+v_{ay}\mathbf{j}+v_{az}\mathbf{k},$$

and a perturber with velocity,

$$\mathbf{v}_p=v_{px}\mathbf{i}+v_{py}\mathbf{j}+v_{pz}\mathbf{k},$$

can be expressed as $W\,dv_{ax}\,dv_{ay}\,dv_{az}\,dv_{px}\,dv_{py}\,dv_{pz}$, where

$$W=\frac{\delta(v_{az}-v_z)}{\pi^{5/2}u_a^2u_p^3}\exp\left(-\frac{(v_{ax}^2+v_{ay}^2)}{u_a^2}-\frac{(v_{px}^2+v_{py}^2+v_{pz}^2)}{u_p^2}\right). \tag{2}$$

Here, u_a and u_p are the most probable speeds in thermal equilibrium for the active molecules and perturbers, respectively. In this study, only self collisions of $^{13}CH_3F$ molecules were studied, so $u_a=u_p=\sqrt{2RT/m}$, where m is the molar mass of $^{13}CH_3F$, R is the gas constant, and T is the temperature. The root-mean-square relative velocity of the colliding molecules calculated with the probability W is

$$\sqrt{\langle v_r^2\rangle}=[\langle(\mathbf{v}_a-\mathbf{v}_p)\cdot(\mathbf{v}_a-\mathbf{v}_p)\rangle]^{1/2}$$
$$=(v_z^2+5RT/m)^{1/2}. \tag{3}$$

Since the relative rms velocity of the colliding molecules is a function of v_z, which is determined by the pump laser offset, it is possible to prepare colliding molecules with different rms relative velocity by changing the pump laser frequency.

B. Velocity change upon collision

In previous studies from this laboratory, a theory has been developed to determine the rms velocity change upon collision for active molecules by analyzing the line shapes of transferred spikes observed in infrared–infrared four-level double resonance.[5–7] The line shapes are analyzed by means of a function based on the Keilson–Storer collision kernel.[17] The final form of the line shape function is a sum of terms of the form $F([\nu-\nu_0]/k)$,[5] where

$$F(v_z)=1/\sqrt{\pi}\beta\int dv_z'f(v_z')\exp\{-[(v_z-\alpha v_z')/\beta]^2\}, \tag{4}$$

in which $f(v_z)$ is the power broadened form,

$$f(v_z)=\frac{\exp[-(v_z/u)^2]}{(\nu_l-\nu_p^0-k_pv_z)^2+\gamma_2^2+\gamma_2x_p^2/\gamma_1}. \tag{5}$$

In these equations, ν and ν_l are the probe and pump laser frequencies, respectively; ν_0 and ν_p^0 are the resonance frequency of the probe and pump transitions, respectively; x_p, γ_1, and γ_2 are the Rabi frequency for the pump, population relaxation rate, and coherence relaxation rate, respectively; $k=\nu_0/c$ and $k_p=\nu_p^0/c$, where c is the speed of light. The constants α and β in the Keilson–Storer collision kernel in Eq. (4) are related by the expression $\alpha^2=1-(\beta/u)^2$, where $0\leqslant\alpha\leqslant1$. The nature of Eq. (4) is such that if $f(v_z')$ is a delta function at $v_z'=v_z''$ then $F(v_z)$ is a Gaussian function centered at $\alpha v_z''$ with half width at half height equal to $\beta(\ln 2)^{1/2}$. Therefore, after collision, the mean value of the component of the velocity in the z direction is $\alpha v_z'$, and the root-mean-square deviation in this component is $\beta/\sqrt{2}$. For the small values of β in this work, $\beta/\sqrt{2}$ is essentially the rms velocity change upon collision. In order to obtain the values of x_p, γ_1, and γ_2, so that Eqs. (4) and (5) can be used, we recorded three-level double resonance spectra under the same experimental conditions as for the four-level double resonance spectra. The three-level double resonance spectra were fit to a theoretical expression derived from a semiclassical treatment, as described in Ref. 30, and the values of x_p, γ_1, and γ_2 which gave the best fit were used for fitting four-level double resonance line shapes.

The line shapes of four-level double resonance spectra were fit to an expression based on Eq. (4) by a least squares method. It was found that a sum of three terms of the form of Eq. (4) represented our experimental line shapes very well. In one of these terms β_i is the limiting value, $\beta_i=u$, in which case $\alpha_i=0$. As mentioned earlier, this term is interpreted as arising from a near resonant swapping of vibrational energy between the active molecule and the perturber. The other two terms are interpreted as representing the results of collisionally-induced direct rotational transitions. The β_i values and the amplitudes of two of the terms, the amplitude of the Gaussian component (the term with $\beta_i=u$), and the center frequency of the probe transition were all adjusted independently by least squares in order to obtain the best fit. The input parameters for the least squares fit include the pump laser offset, the temperature and the values of γ_1, γ_2, and x_p that were determined from the three-level double resonance line shape.

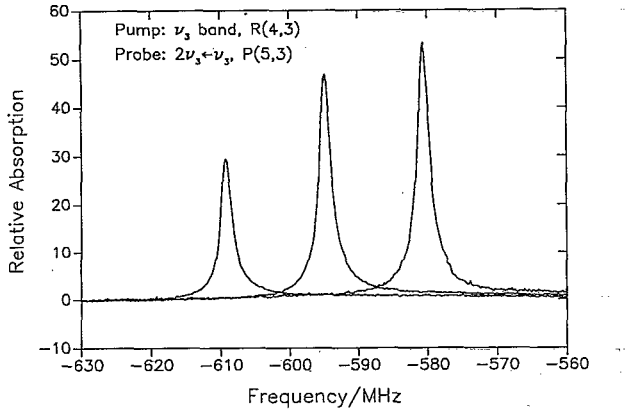

FIG. 3. Comparison of three-level double resonance effects observed with the three different pump laser offsets (37.8, 23.1, and 8.6 MHz from left to right). The lasers used for the pump and probe transitions are given in Table I. The horizontal axis is the probe laser frequency minus 30 093 553.09 MHz; the vertical axis is relative absorption.

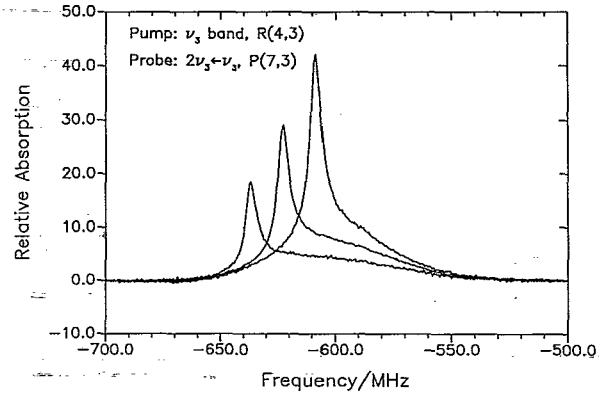

FIG. 4. Comparison of four-level double resonance effects observed with different pump laser offsets (37.8, 23.1, and 8.6 MHz from left to right). The lasers used are given in Table I. The horizontal axis is the probe laser frequency minus 29 988 650.09 MHz; the vertical axis is relative absorption.

IV. RESULTS AND DISCUSSION

A. Three-level double resonance at different pump laser offsets

In the present study, the $^QR(4,3)$ transition in the ν_3 fundamental band of $^{13}CH_3F$ was pumped by the $9P(32)$ $^{12}CO_2$ laser. This laser was known to be coincident with several strong Stark effect transitions in $^{13}CH_3F$ that could be used for stabilization.[31] We chose to lock the pump laser to the Stark Lamb dip of the $^QR(4,1)$, $m=5\leftarrow4$ transition in the ν_3 band of $^{13}CH_3F$. Since the frequency of this transition is easily varied by changing the high voltage applied to the Stark cell, a laser stabilized to this reference can be adjusted to emit at different frequencies within the laser gain curve. By contrast, in conventional fluorescence Lamb dip stabilization, the laser frequency is always at the center of the laser transition.

Three-level double resonance effects in $^{13}CH_3F$ were recorded first to check the frequency stability and the available tunability of the pump laser locked to the Stark Lamb dip. For this purpose, the $^QR(4,3)$ transition in the ν_3 fundamental band was pumped while the $^QP(5,3)$ transition in the $2\nu_3-\nu_3$ hot band was probed. Figure 3 shows a comparison of the double resonance effects observed with three different pump laser offsets. The well-defined line shapes of these Doppler-free spectra indicate that the frequency of the pump laser is extremely stable for all of the pump laser offsets. As mentioned earlier, the velocity component in the direction of the laser beam of the pumped molecules depends on the pump laser offset. When the laser is stabilized to a Stark Lamb dip, the frequency of the laser is generally not known to high accuracy. However, precise values of the pump laser offsets were necessary for analysis of the velocity dependence of the collisionally-induced rotational energy transfer. The Doppler-free feature of the three-level infrared–infrared double resonance line shapes could be used to determine the precise pump laser offsets, provided that the center frequency of the probe transition was known to high accuracy. Fortunately, the frequency of the $^QP(5,3)$ transition in the $2\nu_3-\nu_3$ hot band of $^{13}CH_3F$ has been measured to within ±0.1 MHz in this laboratory.[32] In order to determine the frequencies of the Stark-stabilized pump laser, three-level double resonance spectra at different pump laser offsets were fit to a Lorentz function, and the velocity component was obtained by the counterpart of Eq. (1) for the probe transition. Precise (±0.1 MHz) pump laser offsets determined in this way are listed in Table I.

Three-level double resonance spectra at different pump laser offsets were also used to determine the effective power broadening of the pump transition, $\gamma_2 x_p/\gamma_1$. For this purpose, three or more spectra were recorded at each pump offset for the same pumping power that was used to record four-level double resonance spectra, typically 1 W. The spectra were fit to the three-level double resonance line shape derived from a density matrix formalism, which was discussed in detail in Ref. 30. The values of x_p, γ_1, and γ_2 obtained from the fit were each averaged for different spectra to get the final values that were used to analyze the four-level double resonance line shapes.

B. Initial velocity dependence of the rms velocity change upon collision

As has been shown in the previous work from this laboratory, infrared–infrared four-level double resonance line shapes can provide information about the correlation of rms velocity change and angular momentum change for active molecules as a result of collision. The line shapes obtained with different pump laser offsets allow us to study the velocity dependence of this correlation. For this purpose, we recorded the double resonance effects for each of the $^QP(6,3)$, $^QP(7,3)$, and $^QP(8,3)$ probe transitions in the $2\nu_3-\nu_3$ hot band with three different pump laser offsets (which were the same as those used in three-level double resonance) for the $^QR(4,3)$ pump transition in the ν_3 fundamental band. Figure 4 shows a comparison of the spectra obtained for the $^QP(7,3)$ probe transition. The spectra were analyzed numerically by means of the least squares

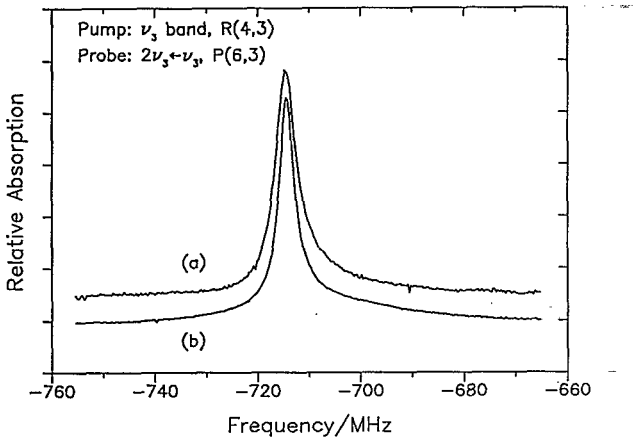

FIG. 5. Comparison of the line shape of the transferred spike observed with pump laser offset at (a) 37.8 MHz (v_z=365.1 m/s) to that at (b) 8.6 MHz (v_z=83.1 m/s); the Gaussian part has been removed from each line shape. The upper spectrum has been shifted in frequency, displaced vertically, and scaled for comparison. The lasers used are given in Table I. The horizontal axis is the probe laser frequency minus 30 041 528.73 MHz; the vertical axis is relative absorption.

fitting program described briefly in Sec. III and in more detail in Ref. 7. It was found that the widths of the transferred spikes were substantially larger for a larger pump laser offset for all of the investigated probe transitions. Figure 5 shows a comparison of the transferred spikes for the $^QP(6,3)$ probe transition in the $2\nu_3-\nu_3$ band while the $^QR(4,3)$ transition in the ν_3 band was pumped at two different pump laser offsets, 8.6 and 37.8 MHz (the spectra have been shifted in frequency, the Gaussian component has been removed, and the intensities have been scaled for the comparison). The upper spectrum was at the larger offset and it is clear that the upper spectrum is wider than the lower one.

Table II summarizes the results obtained from the fittings for the three probed transitions at three different pump laser offsets. The two β parameters in the table were the parameters of the two KS collision kernels that were obtained from the two spike components in each four-level double resonance line shape. Although both of the spike components are interpreted to be the results of direct rotational energy transfer, they are believed to have different origins. The narrower spike component results from molecules that have undergone one or a small number of collisions with a large impact parameter where the intramolecular interaction was weak and the velocity change was small. The broader spike component results from molecules that have undergone either one collision with a small impact parameter, where the intramolecular interaction was strong and the molecular path was deflected with a large angle, or a very large number of collisions with large impact parameters, where the large velocity change was the result of many small changes in velocity during each collision. It is interesting to note in Table II that the value of $\Delta v_{\rm rms}=\beta/\sqrt{2}$, the rms velocity change upon collision, depends on the pump laser offset for both components of the transferred spike for all of the probe transitions examined. The tendency is that the larger the pump laser offset, the larger the rms velocity change.

TABLE II. Transferred spikes for different pumping offsets in $^{13}CH_3F$. Pump transition is $^QR(4,3)$ in the ν_3 fundamental band.

Probe[a]	Pump offset[b]	$k\beta_1$[c]	$(\Delta v_{\rm rms})_1$[d]	$k\beta_2$[e]	$(\Delta v_{\rm rms})_2$[f]
$^QP(6,3)$	8.6	1.22	8.61	7.15	50.5
	23.1	1.35	9.53	8.86	62.5
	37.8	1.52	10.73	10.93	77.1
$^QP(7,3)$	8.6	1.82	12.87	10.44	73.8
	23.1	1.99	14.07	12.20	86.2
	37.8	2.21	15.62	15.98	113.0
$^QP(8,3)$	8.6	2.45	17.35	14.00	99.1
	23.1	2.65	18.77	16.74	118.5
	37.8	2.99	21.17	18.95	134.2

[a]Probe transitions are in the $2\nu_3-\nu_3$ hot band.
[b]Pump laser frequency minus center frequency of the pump transition in MHz.
[c]β_1 is the Keilson–Storer parameter for the narrow spike; k is the magnitude of the wave vector for the probe transition; $k\beta_1$ is in MHz.
[d]Root mean square change in velocity (m/s) for active molecules that contribute to the narrow spike.
[e]β_2 is the Keilson–Storer parameter for the narrow spike; k is the magnitude of the wave vector for the probe transition; $k\beta_2$ is in MHz.
[f]Root-mean-square change in velocity (m/s) for active molecules that contribute to the broad spike.

In the collisional process concerned in this study, the velocity of one molecule of a colliding pair in space fixed coordinates does not determine the nature of collision. What really matters is the relative velocity of the colliding partners. To understand the observed phenomena, we calculated the relative rms velocity of molecules pumped with different pump laser offsets. The dependences of rms velocity change upon collision on the initial relative rms velocity of molecules before collision are summarized in Table III. It is obvious that the rms velocity change is roughly proportional to the initial relative rms velocity of the mol-

TABLE III. Velocity change during state change upon collision in $^{13}CH_3F$.

State change[a]	v_z[b]	v_r[c]	$(\Delta v_{\rm rms})_1$[d]	r_1[e]	$(\Delta v_{\rm rms})_2$[d]	r_2[e]
(5,3)→(6,3)	83.1	599.5	8.61	0.014	50.46	0.08
	223.1	634.3	9.53	0.015	62.52	0.10
	365.1	697.0	10.73	0.015	77.13	0.11
(5,3)→(7,3)	83.1	599.5	12.87	0.021	73.83	0.12
	223.1	634.3	14.07	0.022	86.24	0.14
	365.1	697.0	15.62	0.022	112.96	0.16
(5,3)→(8,3)	83.1	599.5	17.35	0.029	99.14	0.17
	223.1	634.3	18.77	0.030	118.55	0.19
	365.1	697.0	21.17	0.030	134.20	0.19

[a]Rotational state change from (J,K) to (J',K') upon collision in the $v_3=1$ vibrational state.
[b]The z component of the initial velocity of the active molecule before collision (m/s).
[c]Initial root-mean-square relative speed of the colliding molecules $(v_z^2+5u^2/2)^{1/2}$ (m/s); $u=(2RT/M)^{1/2}=375.5$ m/s.
[d]The same as in Table II.
[e]$r_i=(\Delta v_{\rm rms})_i/v_r$ $(i=1,2)$.

TABLE IV. Relative intensities for collisionally-induced transitions in $^{13}CH_3F$.

State change[a]	v_r[b]	A_1/A_2[c]	A_1/A_G[d]	A_2/A_G[e]	R_1[f]	R_2[g]
(5,3)→(6,3)	599.5	1.98	0.59	0.30	1.00	1.00
	697.0	1.94	0.60	0.33	1.06	1.15
(5,3)→(7,3)	599.5	1.21	0.26	0.21	1.00	1.00
	697.0	1.18	0.38	0.34	1.23	1.32
(5,3)→(8,3)	599.5	0.88	0.23	0.25	1.00	1.00
	697.0	0.81	0.33	0.53	1.32	1.86

[a]Rotational state change from (J,K) to (J',K') upon collision in the $v_3=1$ vibrational state.
[b]Initial root mean square relative velocity (m/s) of colliding molecules $(v_z^2+5u^2/2)^{1/2}$ (m/s), $u=(2RT/M)^{1/2}=375.5$ m/s.
[c]The ratio of intensity for the narrow spike to that for the broad spike.
[d]The relative intensity of the narrow spike to the Gaussian in the observed spectrum.
[e]The relative intensity of the broad spike to the Gaussian in the observed spectrum.
[f]The ratio of the intensity of the narrow spike to that at $v_r=599.5$ m/s.
[g]The ratio of the intensity of the broad spike to that at $v_r=599.5$ m/s.

ecules for the same collisionally-induced transition. The proportionality coefficient increases as the change of the J quantum number increases during the collisionally-induced rotational energy transfer.

C. Velocity dependence of rates of energy transfer

While the line width of a spike component in the four-level double resonance line shape contains information about the rms velocity change of the active molecule during rotational energy transfer, the relative intensity of the component reflects the relative rate of the energy transfer process. Comparison of relative intensities of spikes obtained at different pump laser offsets allows us to examine the velocity dependence of the rates for the energy transfer. In previous work from this laboratory,[7] theoretical relations necessary for comparative intensity measurements for four-level double resonance line shapes have been worked out. These theoretical considerations have been built in to the least-squares fitting program, which allowed us to obtain scaled intensities for different components in the observed line shapes. The results are summarized in Table IV.

With the same initial relative rms velocity, the ratio of the area of the narrow component to the broad component of the transferred spikes decreases as ΔJ increases. If the broad component is interpreted as resulting from collisions with small impact parameter, this is an indication that a greater proportion of hard collisions is required for rotational energy transfer with larger ΔJ. For the same ΔJ, the ratio decreases slightly as the initial relative rms velocity increases. This indicates that a collision with a larger relative velocity is harder than that with a smaller velocity.

For the same initial relative rms velocity, the ratios of the areas of both the narrow and the broad components of the transferred spikes to the Gaussian component decrease as ΔJ increases while for the same ΔJ, the ratios increase as the relative rms velocity increases. This indicates that the time required for rotational energy transfer increases as ΔJ increases and that for a larger initial relative velocity a shorter time is required for a rotational energy transfer.

Finally, for the same ΔJ, the intensity of either the narrow or the broad component of the spike is larger at larger relative rms velocity than that at smaller relative rms velocity. The difference is greater as ΔJ increases. The former is understandable since the larger the relative velocity of the colliding molecules, the larger the collisional rate. The latter indicates again that a collision with a larger relative velocity is harder so that it favors a collisionally-induced transition with a large ΔJ.

D. Calculation from classical scattering theory

In Ref. 29 the Monte Carlo method of Borenstein and Lamb[18] was used to calculate classical collision kernels for Lennard-Jones potentials for comparison to the collision kernels derived from transferred spikes recorded by four-level infrared–infrared double resonance. In that work, even though the calculations were performed for elastic scattering with a very simple potential function, it was possible to provide a qualitative interpretation of all of the experimental results obtained by combining the classical calculation with an estimate of the maximum impact parameter for collisionally-induced transition. The estimate of maximum impact parameter was based on the known results of linewidth measurements.

In view of the success obtained with the simple Monte Carlo calculation in Ref. 29, it was natural to compare the experimental results in the present work with calculations for different assumed values of the initial component of the velocity of the active molecule in the direction of the laser beam. In these calculations the initial z component of the velocity (v_z) of the active molecule in a space-fixed coordinate system is fixed, whereas the x and y components of the velocity of the active molecule and the x, y, z components of the velocity of the perturber are all selected randomly from the appropriate Boltzmann distribution. The initial relative coordinates of the perturber, including the impact parameter, are also chosen randomly. The final z component of the velocity of the active molecule in the space-fixed coordinate frame is then calculated by classical scattering theory by means of equations derived by Borenstein and Lamb.[18] The calculation is repeated for many collisions and the final values of the z components of the velocity are collected in bins of width dv_z'. The number of events in each bin at the end of the calculation should be proportional to $W(v_z,v_z')$, where $W(v_z,v_z')dv_z'$ is the probability per unit time that a molecule with initial value v_z has a final value between v_z' and $v_z'+dv_z'$.

As discussed in the earlier work,[29] this procedure suffers from the fact that it is a classical calculation for elastic scattering, whereas our process is inelastic and probably nonclassical. Nevertheless, because the energy and angular momentum change for the collisions of interest here are both small compared to the energy and angular momentum of the collision process, we performed the calculations necessary to make the comparison. Results of the calculation are shown in Fig. 6.

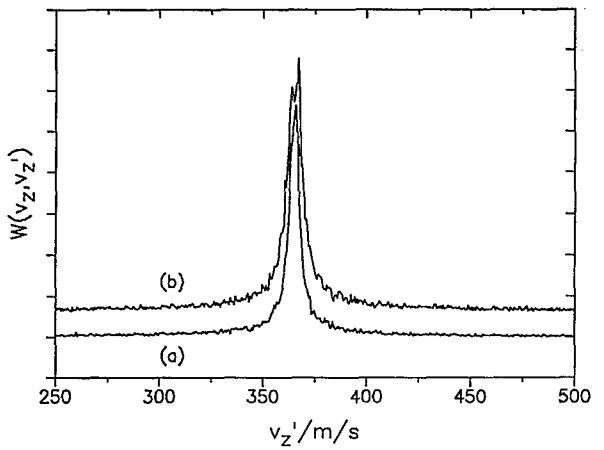

FIG. 6. Comparison of one-dimensional classical collision kernels calculated for two values of the z component of the velocity of the absorber molecule: (a) v_z=365.1 m/s and (b) v_z=83.1 m/s. The Lennard-Jones potential parameters are ε/k_B=300 K and r_e=3.5 Å; the range of impact parameter is $0<b<10$ Å; the mass of the active molecule and the perturber are $35u$; and the number of collisions=20 000. The upper kernel has been shifted in velocity and displaced vertically for comparison. The noise in the plots is sampling noise from the Monte Carlo simulation.

It can be seen from Fig. 6 that the width of the classical collision kernel as a function of the initial v_z of the active molecule is opposite to that of the experiment (Fig. 5). We have performed a similar calculation with the semiclassical scattering equation of Avrillier *et al.*[33] with the same result. Since the failure of the calculated functions to match the experimental curve is almost certainly due to the approximations in the calculation, it may be worth speculating on which aspect of the theory is most responsible for the poor comparison. Our best guess is that the problem is mainly a result of the assumption that the maximum impact parameter is the same at different initial relative velocities. At the higher relative velocities and the same impact parameter, the active molecule and the perturber spend less time in interaction. It is not unreasonable to assume that this leads to a lower probability of collisionally-induced rotational transition for this case. Therefore, it may be expected that the effective maximum impact parameter for induced rotational transition decreases as relative velocity increases. A reduction in maximum impact parameter was shown in Ref. 29 to increase the width of the collision kernel calculated by the Borenstein–Lamb procedure.

Although the interpretation just given explains the discrepancy between Figs. 5 and 6, it should be emphasized that this explanation is highly speculative and it may be that no simple modification of the Monte Carlo procedure employed is useful. The data and trends shown here may have to be interpreted by a quantum mechanical treatment based on inelastic scattering.

V. CONCLUSION

By stabilizing the CO_2 pump laser to a laser Stark Lamb dip, four-level infrared–infrared double resonances in $^{13}CH_3F$ have been recorded at three different pump laser offsets in frequency from the center frequency of the pump transition. The component of the velocity of the molecule in the direction of the pump laser beam is different for each of the laser offsets, and therefore for each offset, collisions with different rms relative velocity of absorber and perturber molecules are probed. Analysis of the line shapes of the double resonances shows that the rms change in velocity for the self-collisions that change the rotational states of $^{13}CH_3F$ molecules increase roughly in direct proportion to the rms relative velocity of the collisions. Theoretical calculations of classical collision kernels for elastic scattering by collisions with limited impact parameter, based on a Lennard-Jones potential function, show the opposite trend. It appears, therefore that the dependence on velocity of rotational energy transfer is not explainable on simple classical mechanical considerations of elastic scattering. Apparently, more sophisticated calculations that include effects of inelasticity and/or quantum effects are needed to explain the velocity dependence.

[1] S. M. Freund, J. W. C. Johns, A. R. W. McKellar, and T. Oka, J. Chem. Phys. **59**, 3445 (1973).
[2] T. W. Meyer and C. K. Rhodes, Phys. Rev. Lett. **32**, 637 (1974); W. K. Bischel and C. K. Rhodes, Phys. Rev. A **14**, 176 (1976).
[3] R. G. Brewer, R. L. Shoemaker, and S. Stenholm, Phys. Rev. Lett. **33**, 63 (1974); R. L. Shoemaker, S. Stenholm, and R. G. Brewer, Phys. Rev. A **10**, 2037 (1974).
[4] J. W. C. Johns, A. R. W. McKellar, T. Oka, and M. Römheld, J. Chem. Phys. **62** 1488 (1975).
[5] Y. Matsuo, S. K. Lee, and R. H. Schwendeman, J. Chem. Phys. **91**, 3948 (1989).
[6] Y. Matsuo and R. H. Schwendeman, J. Chem. Phys. **91**, 3966 (1989).
[7] U. Shin, Q. Song, and R. H. Schwendeman, J. Chem. Phys. **95**, 3964 (1991).
[8] G. Millot, J. Hetzler, G. Pierre, and J. I. Steinfeld, Spectrochim. Acta **45A**, 5 (1989).
[9] J. I. Steinfeld, I. Burak, D. G. Sutton, and A. V. Nowak, J. Chem. Phys. **52**, 5421 (1970).
[10] D. Harradine, B. Foy, L. Laux, M. Dubs, and J. I. Steinfeld, J. Chem. Phys. **81**, 4267 (1984).
[11] B. Foy, L. Laux, S. Kable, and J. I. Steinfeld, Chem. Phys. Lett. **118**, 464 (1985); B. Foy, J. Hetzler, G. Millot, and J. I. Steinfeld, J. Chem. Phys. **88**, 6838 (1988).
[12] T. Oka, J. Chem. Phys. **45**, 754 (1966); **47**, 13 (1967); **47**, 4852 (1967); **48**, 4919 (1968); **49**, 3135 (1968).
[13] T. Oka, Adv. At. Mol. Phys. **9**, 127 (1973).
[14] S. Kano, T. Amano, and T. Shimizu, J. Chem. Phys. **64**, 4711 (1976).
[15] W. A. Kreiner, A. Eyer, and H. Jones, J. Mol. Spectrosc. **52**, 420 (1974).
[16] N. Morita, S. Kano, Y. Ueda, and T. Shimizu, J. Chem. Phys. **66**, 2226 (1977).
[17] J. Keilson and J. E. Storer, Q. Appl. Math. **10**, 243 (1952).
[18] M. Borenstein and W. E. Lamb, Phys. Rev. A **5**, 1311 (1972).
[19] J. Schmidt, P. R. Berman, and R. G. Brewer, Phys. Rev. Lett. **31**, 1103 (1973).
[20] C. Brechignac, R. Vetter, and P. R. Berman, Phys. Rev. A **17**, 1609 (1978).
[21] C. G. Aminoff, J. Javanainen, and M. Kaivola, Phys. Rev. A **28**, 722 (1983).
[22] J. E. M. Haverkort, J. P. Woerdman, and P. R. Berman, Phys. Rev. A **36**, 5251 (1987).
[23] N. Smith, T. A. Brunner, R. D. Driver, and D. E. Pritchard, J. Chem. Phys. **69**, 1498 (1978).
[24] N. Smith, T. A. Brunner, and D. E. Pritchard, J. Chem. Phys. **74**, 467 (1982).
[25] N. Smith, T. P. Scott, and D. E. Pritchard, J. Chem. Phys. **81**, 1229 (1978).
[26] A. T. Mattick, A. Sanchez, N. A. Kurnit, and A. Javan, Appl. Phys. Lett. **23**(12), 675 (1973).

[27] S. B. Grossman, A. Schenzle, and R. G. Brewer, Phys. Rev. Lett. **38**, 275 (1977).
[28] W. H. Weber and R. W. Terhune, Opt. Lett. **6**, 455 (1981).
[29] Q. Song and R. H. Schwendeman, J. Mol. Spectrosc. **153**, 385 (1992).
[30] Q. Song and R. H. Schwendeman, J. Mol. Spectrosc. **149**, 356 (1991).
[31] S. M. Freund, G. Duxbury, M. Römheld, J. T. Tiedje, and T. Oka, J. Mol. Spectrosc. **52**, 38 (1974).
[32] Q. Song and R. H. Schwendeman (unpublished).
[33] S. Avrillier, Ch. J. Borde, J. Picart, and N. T. Minh, J. Phys. **43**, 1213 (1982).